Characterising Bone Material Composition and Structure in the Ovariectomized (OVX) Rat Model of Osteoporosis.

Mathavan, Neashan; Turunen, Mikael J; Tägil, Magnus; Isaksson, Hanna

Published in:
Calcified Tissue International

DOI:
10.1007/s00223-015-9991-7

2015

Characterizing bone material composition and structure in the ovariectomized (OVX) rat model of osteoporosis.

Neashan Mathavan [1]; Mikael J. Turunen [2]; Magnus Tägil [3]; Hanna Isaksson [1,3];

[1] *Department of Biomedical Engineering, Lund University, Sweden.*

[2] *Department of Applied Physics, University of Eastern Finland, Finland.*

[3] *Department of Orthopaedics, Lund University, Sweden.*

Word Count:

Abstract 231 words; Manuscript 4203 words; Figures 6; Tables 1;

Corresponding Author:

Neashan Mathavan, M.Sc.
Department of Biomedical Engineering
Lund University
PO Box 118, 221 00 Lund, SWEDEN
Phone: +46 46 222 06 59
Email: neashan.mathavan@bme.lth.se

Abstract

The ovariectomized (OVX) rat model is well established in investigations of osteoporosis and osteoporotic therapies. Advent of techniques such as Fourier-transform infrared (FTIR) spectroscopy and small angle x-ray scattering (SAXS) facilitate characterization of bone composition and mineral structure, respectively, which are key determinants of bone strength. Limited publications exist on the implementation of these techniques in the OVX rat model. At 12 weeks of age, female Sprague-Dawley rats were either sham operated (n = 6) or ovariectomized (n = 6) and sacrificed 18 weeks later. L2 lumbar vertebrae and proximal tibiae were assessed by μCT, FTIR and SAXS. Presence of extensive trabecular deterioration in the μCT data confirmed the onset of osteoporosis. FTIR compositional parameters were determined including measures of degree of mineralization, crystallinity, collagen maturity and acid phosphate content. Mineral crystal thickness was determined from the SAXS data using two approaches available in literature. Compositionally, a decline in the heterogeneity of acid phosphate content was observed while measures of crystallinity and collagen maturity remained unaltered. Using an iterative curve-fitting method, OVX-induced increases in the mineral crystal thickness of 3.8% and 7.8% ($p < 0.05$) were noted in the trabecular of the vertebra and tibia respectively. In conclusion, implementation of FTIR and SAXS techniques in the OVX rat model, identified no significant compositional changes while substantiating thickening of the mineral crystals as a general structural feature of OVX-induced osteoporosis in rats.

Keywords

osteoporosis; bone composition; bone structure; Fourier-transform infrared spectroscopy FTIR; small angle x-ray scattering SAXS;

Introduction

The ovariectomized (OVX) rat model of postmenopausal osteoporosis is the most widely used animal model to investigate the effects of osteoporosis and is well established in the assessment of osteoporotic therapies [1,2]. Understanding the progression of osteoporosis clinically is typically based on surrogate measures of bone mineral density (BMD). The concept of bone strength, however, contains more qualitative and quantitative aspects than mineral density and new techniques that expand our understanding are warranted. The advent of techniques such as Fourier transform infrared (FTIR) spectroscopy and small angle x-ray scattering (SAXS) in the characterization of bone quality facilitates understanding of osteoporosis from new perspectives. Specifically these techniques contribute to elucidating the significance of bone material composition and nanostructure, respectively, to the mechanical strength of bone and determining how pathogenic perturbations of these properties compromises bone strength. For instance, compositionally, osteoporotic tissue is typically distinguished by a diminished mineral content while structurally ovariectomized monkeys and mice have been noted to exhibit larger crystal sizes, both of which are characteristics coupled to increased bone fragility [3,4]. Thus, our motivation for this study is in identifying compositional and nanostructural changes induced in the OVX rat model using FTIR and SAXS in order to further understand if these changes predispose osteoporotic bone to fractures.

Vibrational spectroscopic techniques, such as FTIR, probe bone composition in normal and diseased states by means of a series of validated spectroscopic parameters, which provide quantitative and qualitative measures of physicochemical properties at discrete anatomical sites. Surprisingly, implementation of FTIR in the OVX rat model has been limited, with only mineral and carbonate content reported in comparisons between healthy/osteoporotic rats [5,6]. A few studies of compositional changes in OVX rat bone have opted for implementation of alternative techniques such as Raman spectroscopy and thermogravimetric or chemical analyses [5,7,8]. Substantial FTIR data does exist for other ovariectomized animal models and humans but the inherent inter-species differences can render direct comparisons problematic.

Use of SAXS in unravelling the nano-scale structural detail of bone is due to its sensitivity to electron density contrast between the mineral crystals and the organic matrix. It entails the transmission of a collimated beam of x-rays through a bone section with the ensuing scattered x-ray intensity recorded at small angles. Measurements can be position-resolved with a resolution similar to that of the beam dimensions. Few publications exist on the implementation of SAXS in the OVX rat model but these are somewhat inconsistent in their findings [9,10,7,11].

The asymmetry of the SAXS scattering pattern of bone is indicative of oriented structures and thus yields orientational parameters quantifying the angular distribution of the mineral crystals [12,13]. Moreover, the characteristic crystal thickness is interpretable from the SAXS intensity spectrum as a function of the scattering intensity, *I(q)*.

Mean mineral crystal thickness has been calculated by two alternative means: The approach set forth by Fratzl et al. is based on the assumption of bone as a two component crystal/matrix composite and evaluates the interfacial area as the ratio of the integrated intensity and the Porod constant, K_P [12,14]. It assumes a mineral phase volume fraction of 50%, which is of questionable validity. Mineral volume fraction of bone is both species and site dependent with documented values varying between 30 to 55% as determined by ash weight/dry weight ratios, energy dispersive x-ray spectroscopy or quantitative backscattered electron imaging [15]. An alternative approach in determining the mean crystal thickness parameter is that suggested by Bünger et al., which relies on iterative curve fitting to the radially averaged one dimensional SAXS pattern *I(q)* [10]. Significantly, this method is independent of any assumptions on bone mineral content. Limited adoption of iterative curve fitting exists in the literature with, to our knowledge, only a sole publication on its implementation in the OVX rat model [10]. However, this study was restricted to a sample size of n = 3 [10].

Our aim in this study was to use FTIR and SAXS to investigate the underlying alterations in bone composition and structure between healthy and OVX rats. In particular, this study applied FTIR in the characterization of compositional changes in osteoporotic bone through the inclusion of previously unreported spectral parameters. Moreover, this study investigated changes in mineral crystal thickness in a statistically relevant sample size using the curve fitting approach. As no previous study has presented a comparison of the Fratzl and curve fitting methods, and given that the few studies that have reported on the mineral thickness parameter in the OVX rat model have been conflicting, this study implemented both methods in the interests of extracting comprehensive and conclusive results on the changes induced by ovariectomy.

Materials and Methods

Experimental protocol

12 female Sprague-Dawley (Charles River, Germany) rats were randomly assigned to two groups of equal size. At 12 weeks, one group was sham-operated on and the second group was ovariectomized. The rats were sacrificed 18

weeks later and the tibiae and L2 lumbar vertebral bodies were harvested. Body weight at time point of sacrifice was 352 ± 22 g and 397 ± 19 g for sham-operated and ovariectomized rats, respectively. Bones from all rats were assessed by μCT, FTIR and SAXS. Ethical approval of care and experimental protocol was obtained from the local animal ethics and scientific advisory committee (Ethical Permission No. M316-11).

μCT

The L2 lumbar vertebral body and proximal tibia of each rat were imaged with Skyscan 1172 (v. 1.5, Bruker, Belgium), using an isotropic voxel size of 15 μm. Images were acquired using x-ray source settings of 100 kV/100 μA, 8 repeated scans and the use of a 0.5 mm aluminium filter for noise reduction. Image reconstruction was performed with NRecon (Skyscan, v 1.5.1.4). Optimal corrections for ring artefacts and beam hardening were applied. Regions of interest (ROIs) comprised the complete trabeculae architecture of the lumbar vertebral body and the proximal epiphysis of the tibiae, respectively (Figure 1A, 1B). In addition, a volume within the proximal metaphysis extending 1.5 mm distally from the growth plate was also evaluated (Figure 1C). ROIs were defined via a semi-automated process wherein the user draws 2D ROIs at specific images throughout the images, which are then extrapolated across all intervening images using a dynamic interpolation algorithm in CTAn (Skyscan, v 1.9.3.2).

Images were globally thresholded at 44% of the maximum gray value with the segmentation threshold determined based on visual comparison of the grayscale image and the threshold at which the resulting binary image most closely represented the original image (CTAn, v. 1.9.3.2 Skyscan, Belgium). The following bone microstructural parameters were quantified: trabecular thickness (Tb.Th), trabecular number (Tb.N), trabecular separation (Tb.Sp), bone volume fraction (BV/TV), structure model index (SMI) and degree of anisotropy (DA). Following μCT, the L2 vertebral bodies and tibiae were fixed with 4% formaldehyde, progressively dehydrated, and finally embedded in epoxy resin.

FTIR

Tibial sections (4 μm) were cut using a HM 355S microtome (Thermo Scientific, Mass.) and transferred onto BaF_2 windows. FTIR measurements were conducted at the D7 beamline of the MAX-IV laboratory (Lund, Sweden). Spectral acquisition was performed in transmission mode using a Bruker 66V FTIR spectrometer coupled to a

Bruker Hyperion 3000 IR microscope (Bruker Corp., Mass.) at a spatial resolution of 10 μm, spectral resolution of 4 cm^{-1} and 64 repeated scans. Collected wavelengths ranged from 2000 - 800 cm^{-1}. Spectra in 50 x 50 μm areas (steps of 10μm, resulting in 36 spectra) of cortical and trabecular bone in the proximal epiphysis of each tibia were recorded along with a reference spectrum of epoxy resin. Acquired spectra were subsequently baseline corrected and the spectral contribution of epoxy resin was subtracted [16,17]. The following spectroscopic parameters were calculated using custom-written scripts in MATLAB: mineral-matrix ratio (1200 – 900 cm^{-1} / 1720 – 1585 cm^{-1}) [18], carbonate-phosphate ratio (890 – 850 cm^{-1} / 1200 – 900 cm^{-1}) [19], crystallinity (1030/1020 cm^{-1}) [20,21], collagen maturity (1660/1690 cm^{-1}) [22] and acid phosphate (1127/1096 cm^{-1}) [23]. Furthermore, the spatial heterogeneity of each parameter was determined from the full width of half maximum (FWHM) of the Gaussian curve fitted to the pixel histogram of the measured area [24].

SAXS

Sections of 400 μm thickness were obtained from the L2 vertebrae and tibiae using a low-speed, water-cooled IsoMet 11-1180 saw (Buehler, Illinois) with a diamond blade. Small angle x-ray scattering (SAXS) measurements were conducted at the I911-4 beamline of the MAX IV synchrotron facility (Lund, Sweden) [25]. A 1 x 2 mm region of the trabecular bone from the L2 lumbar vertebra and the metaphysis of the proximal tibia were scanned. Sections were scanned with a beam size of 0.1 x 0.1 mm with a 0.1 mm step size. A scattering image was obtained at each position using an exposure time of 15 s (λ = 0.91 Å, q-range 0.01 - 0.30 $Å^{-1}$). Pre-processing of the SAXS images entailed masking away the beam stop and peripheral regions adjacent to the detector area. Subsequently, SAXS parameters were determined from the scattered intensity spectrum, I(q, Ψ), using custom-written scripts for each measurement point as described below [17].

Calculation of orientational parameters were obtained by fitting Gaussian curves to the two symmetrical peaks of the azimuthal dependence of the q-integrated scattered intensity I(Ψ) and follow the methodology described in our previous publication [17].

Calculation of mean crystal thickness from the azimuthally averaged SAXS intensity spectrum as a function of the scattering angle, I(q), was achieved using two approaches. The Fratzl approach relies on obtaining the Porod

constant, K_P, by fitting the expression K_P/q^4 to the I(q) data at high q ranges where the scattering profile of any particle system decays [12,14]. The following expression then yields the thickness parameter *T* based on the assumption that the particles are plate-shaped,

$$T = \frac{4}{\pi K_P} \int_{q_{min}}^{q_{max}} I(q) q^2 \, dq \tag{1}$$

The alternative approach in extracting the characteristic particle thickness adopts iterative curve fitting to the I(q) profile [10]. Dimensions of the mineral crystals are assumed to be of finite thickness, *T*, along one dimension and infinite in the other two dimensions, i.e. plate-shaped crystals. In brief, the average scattering is expressed as,

$$P_{avg} = \frac{\int_0^\infty T^2 \, P(q) \; D\left(T, T_{avg}\right) dT}{\int_0^\infty T^2 \, D(T, T_{avg}) \, dT} \tag{2}$$

where a Schultz-Zimm distribution $D\left(T, T_{avg}\right)$ is assumed to account for a distribution in crystal thickness. Expanding on equation (2) to consider interparticle interactions of neighbouring particles necessitates the inclusion of a structure factor. As formulated by Bünger et al. short-range order repulsions are accounted for by use of the random phase approximation (RPA),

$$S_{RPA}(q) = \frac{1}{1 + \nu P_{avg}(q)} \tag{3}$$

where ν is an adaptable parameter that is dependent on interaction strength which in turn is positively correlated to particle concentration. Further factoring in the presence of excess scattering at low q due to long-range order electron density inhomogeneities with the following expression,

$$S_{frac}(q) = 1 + Aq^{-\alpha} \tag{4}$$

where α corresponds to the fractal dimension of the fluctuations. Thus, the model describing the total intensity, $I(q)$, is,

$$I(q) = CS_{frac}(q)S_{RPA}(q)P_{avg}(q) \quad (5)$$

where C is a scale factor dependent on specimen thickness, mineral content and scattering contrast [10]. Subsequently, custom-written MATLAB scripts automated the iterative weighted nonlinear least squares fitting of the model to the measured data (MATLAB R2010b, The Mathworks Inc, MA, USA) with suitable initial values selected for the parameters (Figure 2) [17].

Statistics

The Mann-Whitney U-test was used for comparisons between the Control and OVX groups for all measurement parameters (SPSS, v22, SPSS Inc). The Wilcoxon signed rank test was used to compare trabecular and cortical composition within Control and OVX groups (SPSS, v22, SPSS Inc).

Results

µCT

Overall, substantial deterioration of the trabeculae was evident when comparing control and OVX bone microstructure (Figure 3). Significant decreases in BV/TV were observed in the trabeculae of the tibial epiphysis (-17%; $p < 0.01$), tibial metaphysis (-50%; $p < 0.01$) and the lumbar vertebrae (-26%; $p < 0.05$) (Figure 4A). Concurrently, in the vertebrae and in the tibial epiphysis and metaphysis, this was associated with significant decreases in Tb.N of 27%, 22% and 59% respectively ($p < 0.01$) (Figure 4B) and significant increases in Tb.Sp of 24%, 20% and 177% respectively ($p < 0.05$; $p < 0.01$; $p < 0.01$) (Figure 4C). A significant thickening of the trabeculae was observed in the metaphysis of the tibiae (+21%; $p < 0.01$) (Figure 4D). Furthermore, a shift in the SMI was observed from plate-like trabeculae to rod-like trabeculae for all three sets of data ($p < 0.05$; $p < 0.01$; $p < 0.01$) (Figure 4E). No alterations in the DA was present at any site (Figure 4F).

FTIR

Small but non-significant differences were observed between Control and OVX groups in relation to degree of mineralization and acid phosphate content. Moreover, these differences were more pronounced in the trabeculae than in the cortices (Figure 5). Mineral-matrix ratio in the OVX rats exhibited decreases of -7.5% in trabecular bone and -

5.8**%** in cortical bone relative to Control rats (Figure 5A). A reduction in acid phosphate content of -4.6% in trabecular bone and -3.3% in cortical bone was also noted in the OVX group (Figure 5C). Furthermore, when considering the heterogeneity in spectroscopic parameters, the OVX group recorded a significantly lower variation for the acid phosphate content parameter than the Control group ($p < 0.05$). Irrespective of the underlying bone health, trabecular composition exhibited significantly lower mineral content, carbonate substitution and crystallinity relative to cortices ($p < 0.05$), while acid phosphate presence and collagen maturity were similar (Figure 5).

SAXS

Computation of the mean mineral crystal thickness underscored a small increase induced by OVX at both bone sites. This increase was particularly pronounced with the curve fitting method where increases of 3.8% and 7.8% were noted in the vertebra and tibia ($p < 0.05$) respectively (Figure 6). The magnitude of this thickening was smaller using the Fratzl method. In both approaches, these increases reached statistical significance in the proximal tibial metaphysis ($p < 0.05$) but not so in the vertebrae (Figure 6). In general, larger variation in the measurements was observed with the fitted method than the Fratzl method. Only in the tibia did these variations significantly differ between Control (0.055 nm) and OVX (0.23 nm) groups ($p < 0.05$). Site specific comparisons showed that the mineral crystal thickness was significantly higher in the trabecula of the vertebra than in the tibia ($p < 0.05$ for both healthy and osteoporotic rats, Figure 6). No differences were noted in the orientational parameters (Table 1).

Discussion

Determining the influence of composition and structure on bone strength in healthy and diseased states are critical in the development of treatments for conditions such as osteoporosis. Implementation of FTIR and SAXS in the present study addresses the compositional and structural changes in osteoporotic bone in the OVX rat model. Findings are presented of induced structural changes in the thickening of the mineral crystals, while compositionally a decline in the heterogeneity of the acid phosphate content is observed without any alteration in the crystallinity and collagen maturity measures.

Morphological changes and their time-dependence in the trabecular bone structure as a consequence of OVX have been extensively documented based on μCT analysis for both the vertebrae and tibia in rats [26-28]. Our observed declines in BV/TV and Tb.N, and a shift from plate-like trabeculae to rod-like trabeculae are in line with

previous publications and confirms the onset of ovariectomy-induced osteoporosis [26-28]. One exception to the published literature is the finding of an increase in the Tb.Th parameter in one of the three analyzed regions, i.e. the proximal metaphyseal tibia. Previous studies have reported either a decrease or no-change. It is possible this is an anomaly given the small sample size in our study. Alternatively, it is possible that if many thin trabeculae are completely resorbed (as suggested by our data), then an increase in the remaining average Tb.Th could be observed.

Analyses based on infrared spectroscopy have previously characterized the differences between healthy and osteoporotic bone in humans [3]. Compared with healthy bone, osteoporotic bone has been suggested to have lower mineral content [29,30] with a few reported exceptions using non-spectroscopic methods [31-33], unchanged acid phosphate content [34] and augmented mineral crystallinity [30,35], carbonate content [30,34] and collagen maturity [36].

In this study, spectral analysis of osteoporotic bone in the OVX rat model showed a trend towards a diminished mineral content level, albeit not to a statistically significant degree. In a previously published study by Bohic et al., 6.5 month old rats were ovariectomized and sacrificed at 1 year post-surgery [5]. Spectral analysis comprised two parameters: the mineral-matrix ratio and the carbonate-phosphate ratio. A significant decrease ($p < 0.05$) was observed in the OVX group relative to the Control group for the mineral-matrix ratio. The rats in this instance were older at the time-point of sacrifice than in the current study (78 weeks vs 30 weeks) and it stands to reason that the differences observed in our study would be more pronounced at a similar time-point further along.

Consistent with previously reported comparisons in humans, acid phosphate content levels were similar in Control and OVX groups. However, the heterogeneity of the acid phosphate parameter in our data was noted to be significantly less in osteoporotic samples. This is indicative of the limited presence of new bone deposition and is in line with expectations of the changes induced by osteoporosis. While changes in acid phosphate content (or its heterogeneity) have not been observed in human osteoporotic bone, it is important to note however that the parameter used as a measure of acid phosphate substitution in this study, 1127/1096 cm^{-1}, was identified recently and its implementation has not been reported extensively [23].

Mineral crystal thickness values obtained in this study for healthy rats are in line with previous publications using both the fitted and Fratzl methods [10,12,14]. Two other studies have also reported increased mineral crystal thickness induced by OVX. Valenta et al reported increases in the trabeculae (7%; $p < 0.05$), midshaft cortex (3%) and metaphyseal cortex (5%; $p < 0.05$) of the distal femur at 94 weeks of age using the Fratzl method [9]. This compares well to our findings of an increase of 4.5% ($p < 0.05$) in the trabeculae of the proximal metaphyseal tibiae observed in this study at 30 weeks using the Fratzl method. Rat breed and time-point of ovariectomy were identical in both studies and only differing in the bone sites investigated. Thus, together our findings are suggestive of gradual thickening of the mineral crystals over time. A second study reported values derived with the use of the iterative fitting method but in limited sample numbers: a single cortical bone site in 3 healthy and 3 OVX rats [10]. In presenting their results, the authors made a distinction between newly-formed and old bone and reported an increase of 4.6% in new bone and no change in old bone at 44 weeks of age. Findings in our study with the iterative fitting method are more conclusive with increases of 3.8% and 7.8% ($p < 0.05$) measured at 30 weeks of age (18 weeks post-OVX) in the vertebra and tibia respectively.

The fitted method is, arguably, more representative of the changes induced by OVX. As previously described, the Fratzl method is based on the assumption that the volume fraction of the mineral phase is 50%. Architectural motifs such as trabeculae and osteons which form the structural basis of cancellous and cortical bone respectively, exhibit pronounced local variation in mineral volume fraction ranging from 0 to 43% in humans [15]. A solution adopted in some studies to circumvent this assumption in the Fratzl method has been to independently determine the volume fraction using quantitative backscattered electron imaging (qBEI) [37]. However, at issue also is the dependence of the derivation of the Porod constant on fitting the expression K_P/q^4 to the scattered intensity at high-q values where the signal fades and is progressively indistinguishable from background and noise contributions. Furthermore, the accuracy of the integral intensity is similarly compromised by the necessity of having to extrapolate the scattered intensity profile asymptotically at high-q regions where no experimental data is available. The fitted method avoids these pitfalls as it is independent of assumptions on mineral content and is less influenced by the degradation in the signal quality at high-q values since a broader range of the *I(q)* curve is fitted. It should be noted that there are some uncertainties with the fitted method in factoring in the positional correlation between particles but in the absence of contradictory evidence, it is arguably acceptable.

Noteworthy also are two separate publications in the literature which do not demonstrate significant differences in crystal thickness following ovariectomy [7,11]. Naturally, disparities in reported values can be attributable to a multitude of factors ranging from rat breed, anatomical sites investigated to time-points of ovariectomy and/or sacrifice. Both studies reported values in the region of expected magnitude utilizing the Fratzl approach. In the case of Huang et al., the absence of significant difference is likely a consequence of having a time duration of only 12 weeks between ovariectomy and point of sacrifice, the shortest of any of the studies published [7]. Similarly, the most questionable aspect of the conclusions drawn by Yao et al. is the restriction of sample numbers to n = 4 which obviously makes statistical comparison challenging [11].

Certainly, the magnitude of the thickening in the crystals reported in our study is relatively small and is likely due to the collagen matrix confining the growth in thickness. Neutron scattering experiments in adult bovine samples corroborate this premise with the radial distance between collagen molecules in wet mineralized bone measured to be 1.24 nm which is substantially lower compared to the 1.53 nm measured in wet demineralized bone [38]. This suggests that, in the absence of external macroscopic volume changes, the collagen matrix has to compress to accommodate the growth of the mineral crystals.

Furthermore, minor growth in mineral crystal thickness is to be expected, as it is consistent with the processes in effect during aging and osteoporosis. Foremost, as demonstrated by Roschger et al. in a study of human L4 lumbar vertebral bodies ranging in age from 15 weeks post conception to 97 years of age, is the existence of a highly linear correlation between mineral crystal thickness and the logarithm of average age [39]. This age-dependency translates as a characteristic time course marked by rapid growth in early development (i.e. primary mineralization), and much slower growth thereafter (i.e. secondary mineralization). Similar observations were also reproduced in a study of mice and rats [40].

Significant site-specific variations in mean crystal thickness such as the values obtained for the L2 lumbar vertebrae and tibial metaphyses (Figure 6) can be attributed to the coupled effects of age-dependent mineralization and bone remodelling. Bone remodelling is the continuous, coordinated process by which mature bone is resorbed

and then re-synthesized and thereby primary mineralization begins anew. Studies have demonstrated, through the use of quantitative backscattered electron imaging (qBEI), the quantitative mapping of the distinct local variation in mineral content as a consequence of these coupled molecular mechanisms at work [15].

Moreover, it can be inferred that the disparities in average crystal thickness between age-matched healthy and osteoporotic bone, as presented in this study, are a result of upregulated but imbalanced bone remodelling associated with postmenopausal osteoporosis which favours bone resorption [41]. Indeed, Valenta et al reported a measure of mineralization homogeneity between control and OVX trabeculae based on analysis of qBEI data [9]. Their results were indicative of greater homogeneity in mineralization and accordingly, an overall higher maturity of OVX trabeculae relative to controls. Interestingly, contradicting this notion of higher maturity, we noted significantly higher variation in the Fitted thickness parameter for the OVX tibia samples relative to controls.

Of relevance in the interpretation of our overall findings is that the combinations of age, anatomical sites and time post-OVX are significant factors in the extent of structural and compositional changes present. Moreover, limitations of the study also arise from the small number of rats in each group (n = 6) and the use of a single time-point (30 weeks) for evaluation. However, with respect to use of techniques that requires large scale synchrotron facilities, a group size of 6 is not unreasonably small.

In conclusion, our findings in the bone of ovariectomized rats at 30 weeks show extensive trabecular deterioration, increased mineral crystal thickness and indications of osteoporosis-related compositional changes which, in the absence of significant differences, are not conclusive. In contrast to the extensive use of the OVX rat model in literature, there is only a very sparse presence of studies of compositional and structural changes and thus the findings presented herein represent a significant contribution in elucidating the deterioration in bone quality induced by osteoporosis.

Acknowledgements

Funding for this study from the European Commission (FRACQUAL-293434) and the Swedish Governmental Agency for Innovation Systems (VINNOVA) is acknowledged. Beamtime was generously granted at the I911-SAXS

beamline and the D7 beamline at MAX IV Laboratory, Lund, Sweden. The authors would also like to gratefully acknowledge the technical assistance of Mea Pelkonen, Ana Labrador (I911-SAXS beamline) and Anders Engdahl (D7 beamline).

Conflict of Interest

Authors Neashan Mathavan, Mikael J. Turunen, Magnus Tägil and Hanna Isaksson declare that they have no conflict of interest.

Ethical approval

All procedures performed in this study were in accordance with the ethical standards of Lund University, Sweden, where the study was conducted. All institutional and national guidelines for the care and use of laboratory animals were followed.

References:

1. Bagi CM, Wilkie D, Georgelos K, Williams D, Bertolini D (1997) Morphological and structural characteristics of the proximal femur in human and rat. Bone 21 (3):261-267. doi:http://dx.doi.org/10.1016/S8756-3282(97)00121-X
2. Kalu DN (1991) The ovariectomized rat model of postmenopausal bone loss. Bone and Mineral 15 (3):175-191. doi:http://dx.doi.org/10.1016/0169-6009(91)90124-I
3. Faibish D, Ott SM, Boskey AL (2006) Mineral Changes in Osteoporosis: A Review. Clinical Orthopaedics and Related Research 443:28-38 10.1097/1001.blo.0000200241.0000214684.0000200244e
4. Boskey A (2003) Bone mineral crystal size. Osteoporosis international : a journal established as result of cooperation between the European Foundation for Osteoporosis and the National Osteoporosis Foundation of the USA 14 Suppl 5:S16-20; discussion S20-11
5. Bohic S, Rey C, Legrand A, Sfihi H, Rohanizadeh R, Martel C, Barbier A, Daculsi G (2000) Characterization of the trabecular rat bone mineral: effect of ovariectomy and bisphosphonate treatment. Bone 26 (4):341-348. doi:http://dx.doi.org/10.1016/S8756-3282(99)00276-8
6. Ouyang H, Sherman PJ, Paschalis EP, Boskey AL, Mendelsohn R (2004) Fourier Transform Infrared Microscopic Imaging: Effects of Estrogen and Estrogen Deficiency on Fracture Healing in Rat Femurs. Applied Spectroscopy 58 (1):1-9. doi:10.1366/000370204322729405
7. Huang J, Wang X, Zhang T-L, Wang K (2009) Alterations of ovariectomized rat bone and impact of non-collagenous proteins on mineralization. Joint Bone Spine 76 (2):176-183. doi:http://dx.doi.org/10.1016/j.jbspin.2008.04.017
8. Akkus O, Adar F, Schaffler MB (2004) Age-related changes in physicochemical properties of mineral crystals are related to impaired mechanical function of cortical bone. Bone 34 (3):443-453. doi:http://dx.doi.org/10.1016/j.bone.2003.11.003
9. Valenta A, Roschger P, Fratzl-Zelman N, Kostenuik PJ, Dunstan CR, Fratzl P, Klaushofer K (2005) Combined treatment with PTH (1 - 34) and OPG increases bone volume and uniformity of mineralization in aged ovariectomized rats. Bone 37 (1):87-95
10. Bünger M, Oxlund H, Hansen T, Sørensen S, Bibby B, Thomsen J, Langdahl B, Besenbacher F, Pedersen J, Birkedal H (2010) Strontium and Bone Nanostructure in Normal and Ovariectomized Rats Investigated by Scanning Small-Angle X-Ray Scattering. Calcified Tissue International 86 (4):294-306. doi:10.1007/s00223-010-9341-8
11. Yao W, Cheng Z, Koester KJ, Ager JW, Balooch M, Pham A, Chefo S, Busse C, Ritchie RO, Lane NE (2007) The degree of bone mineralization is maintained with single intravenous bisphosphonates in aged estrogen-deficient rats and is a strong predictor of bone strength. Bone 41 (5):804-812. doi:http://dx.doi.org/10.1016/j.bone.2007.06.021
12. Fratzl P, Schreiber S, Klaushofer K (1996) Bone Mineralization as Studied by Small-Angle X-Ray Scattering. Connective Tissue Research 34 (4):247-254. doi:doi:10.3109/03008209609005268
13. Fratzl P, Paris O, Klaushofer K, Landis WJ (1996) Bone mineralization in an osteogenesis imperfecta mouse model studied by small-angle x-ray scattering. The Journal of Clinical Investigation 97 (2):396-402
14. Rinnerthaler S, Roschger P, Jakob HF, Nader A, Klaushofer K, Fratzl P (1999) Scanning Small Angle X-ray Scattering Analysis of Human Bone Sections. Calcified Tissue International 64 (5):422-429. doi:10.1007/pl00005824
15. Fratzl P, Gupta H, Paschalis E, Roschger P (2004) Structure and mechanical quality of the collagen–mineral nano-composite in bone. Journal of Materials Chemistry 14 (14):2115-2123
16. Isaksson H, Turunen MJ, Rieppo L, Saarakkala S, Tamminen IS, Rieppo J, Kröger H, Jurvelin JS (2010) Infrared spectroscopy indicates altered bone turnover and remodeling activity in renal osteodystrophy. Journal of Bone and Mineral Research 25 (6):1360-1366. doi:10.1002/jbmr.10

17. Turunen MJ, Lages S, Labrador A, Olsson U, Tägil M, Jurvelin JS, Isaksson H (2014) Evaluation of composition and mineral structure of callus tissue in rat femoral fracture. Journal of Biomedical Optics 19 (2):025003-025003. doi:10.1117/1.JBO.19.2.025003
18. Boskey A, Pleshko Camacho N (2007) FT-IR imaging of native and tissue-engineered bone and cartilage. Biomaterials 28 (15):2465-2478. doi:http://dx.doi.org/10.1016/j.biomaterials.2006.11.043
19. Rey C, Collins B, Goehl T, Dickson I, Glimcher M (1989) The carbonate environment in bone mineral: a resolution-enhanced Fourier transform infrared spectroscopy study. Calcified tissue international 45 (3):157-164
20. Pleshko N, Boskey A, Mendelsohn R (1991) Novel infrared spectroscopic method for the determination of crystallinity of hydroxyapatite minerals. Biophysical Journal 60 (4):786-793
21. Gadaleta SJ, Paschalis EP, Betts F, Mendelsohn R, Boskey AL (1996) Fourier transform infrared spectroscopy of the solution-mediated conversion of amorphous calcium phosphate to hydroxyapatite: New correlations between X-ray diffraction and infrared data. Calcified Tissue International 58 (1):9-16. doi:10.1007/BF02509540
22. Paschalis EP, Verdelis K, Doty SB, Boskey AL, Mendelsohn R, Yamauchi M (2001) Spectroscopic Characterization of Collagen Cross-Links in Bone. Journal of Bone and Mineral Research 16 (10):1821-1828. doi:10.1359/jbmr.2001.16.10.1821
23. Spevak L, Flach C, Hunter T, Mendelsohn R, Boskey A (2013) Fourier Transform Infrared Spectroscopic Imaging Parameters Describing Acid Phosphate Substitution in Biologic Hydroxyapatite. Calcified Tissue International:1-11. doi:10.1007/s00223-013-9695-9
24. Turunen MJ, Saarakkala S, Helminen HJ, Jurvelin JS, Isaksson H (2011) Age-related changes in organization and content of the collagen matrix in rabbit cortical bone. Journal of Orthopaedic Research 30 (3):435-442. doi:10.1002/jor.21538
25. Labrador A, Cerenius Y, Svensson C, Theodor K, Plivelic T The yellow mini-hutch for SAXS experiments at MAX IV Laboratory. In: Journal of Physics: Conference Series, 2013. vol 7. IOP Publishing, p 072019
26. Boyd SK, Davison P, MÃ¼ller R, Gasser JrA (2006) Monitoring individual morphological changes over time in ovariectomized rats by in vivo micro-computed tomography. Bone 39 (4):854-862
27. Maïmoun L, Brennan-Speranza TC, Rizzoli R, Ammann P (2012) Effects of ovariectomy on the changes in microarchitecture and material level properties in response to hind leg disuse in female rats. Bone (0)
28. Brouwers JEM, Lambers FM, van Rietbergen B, Ito K, Huiskes R (2009) Comparison of bone loss induced by ovariectomy and neurectomy in rats analyzed by in vivo micro-CT. Journal of Orthopaedic Research 27 (11):1521-1527. doi:10.1002/jor.20913
29. Boskey A, Mendelsohn R (2005) Infrared analysis of bone in health and disease. Journal of biomedical optics 10 (3):031102
30. Gadeleta SJ, Boskey AL, Paschalis E, Carlson C, Menschik F, Baldini T, Peterson M, Rimnac CM (2000) A physical, chemical, and mechanical study of lumbar vertebrae from normal, ovariectomized, and nandrolone decanoate-treated cynomolgus monkeys (macaca fascicularis). Bone 27 (4):541-550. doi:http://dx.doi.org/10.1016/S8756-3282(00)00362-8
31. Busse B, Hahn M, Soltau M, Zustin J, Püschel K, Duda GN, Amling M (2009) Increased calcium content and inhomogeneity of mineralization render bone toughness in osteoporosis: Mineralization, morphology and biomechanics of human single trabeculae. Bone 45 (6):1034-1043. doi:http://dx.doi.org/10.1016/j.bone.2009.08.002
32. Boyde A, Compston JE, Reeve J, Bell KL, Noble BS, Jones SJ, Loveridge N (1998) Effect of estrogen suppression on the mineralization density of iliac crest biopsies in young women as assessed by backscattered electron imaging. Bone 22 (3):241-250. doi:http://dx.doi.org/10.1016/S8756-3282(97)00275-5

33. Koehne T, Vettorazzi E, Küsters N, Lüneburg R, Kahl-Nieke B, Püschel K, Amling M, Busse B (2014) Trends in trabecular architecture and bone mineral density distribution in 152 individuals aged 30–90 years. Bone 66 (0):31-38. doi:http://dx.doi.org/10.1016/j.bone.2014.05.010
34. Boskey AL, DiCarlo E, Paschalis E, West P, Mendelsohn R (2005) Comparison of mineral quality and quantity in iliac crest biopsies from high- and low-turnover osteoporosis: an FT-IR microspectroscopic investigation. Osteoporosis International 16 (12):2031-2038. doi:10.1007/s00198-005-1992-3
35. Paschalis EP, Betts F, DiCarlo E, Mendelsohn R, Boskey AL (1997) FTIR Microspectroscopic Analysis of Human Iliac Crest Biopsies from Untreated Osteoporotic Bone. Calcified Tissue International 61 (6):487-492. doi:10.1007/s002239900372
36. Paschalis EP, Shane E, Lyritis G, Skarantavos G, Mendelsohn R, Boskey AL (2004) Bone Fragility and Collagen Cross-Links. Journal of Bone and Mineral Research 19 (12):2000-2004. doi:10.1359/jbmr.040820
37. Zizak I, Roschger P, Paris O, Misof BM, Berzlanovich A, Bernstorff S, Amenitsch H, Klaushofer K, Fratzl P (2003) Characteristics of mineral particles in the human bone/cartilage interface. Journal of Structural Biology 141 (3):208-217. doi:http://dx.doi.org/10.1016/S1047-8477(02)00635-4
38. Bonar LC, Lees S, Mook HA (1985) Neutron diffraction studies of collagen in fully mineralized bone. Journal of Molecular Biology 181 (2):265-270. doi:http://dx.doi.org/10.1016/0022-2836(85)90090-7
39. Roschger P, Grabner BM, Rinnerthaler S, Tesch W, Kneissel M, Berzlanovich A, Klaushofer K, Fratzl P (2001) Structural Development of the Mineralized Tissue in the Human L4 Vertebral Body. Journal of Structural Biology 136 (2):126-136
40. Fratzl P, Fratzl-Zelman N, Klaushofer K, Vogl G, Koller K (1991) Nucleation and growth of mineral crystals in bone studied by small-angle X-ray scattering. Calcified Tissue International 48 (6):407-413. doi:10.1007/BF02556454
41. Feng X, McDonald JM (2011) Disorders of bone remodeling. Annual review of pathology 6:121

Figure 1. Regions of interest (ROIs) in the lumbar vertebral body [A], proximal epiphysis [B] and proximal metaphysis [C] of the tibia for microCT morphological analysis. In the case of [A] and [B], the complete trabecula architecture was extracted. In the case of [C] the ROI was defined by a volume extending a distance of 1.5 mm distal to the growth plate.

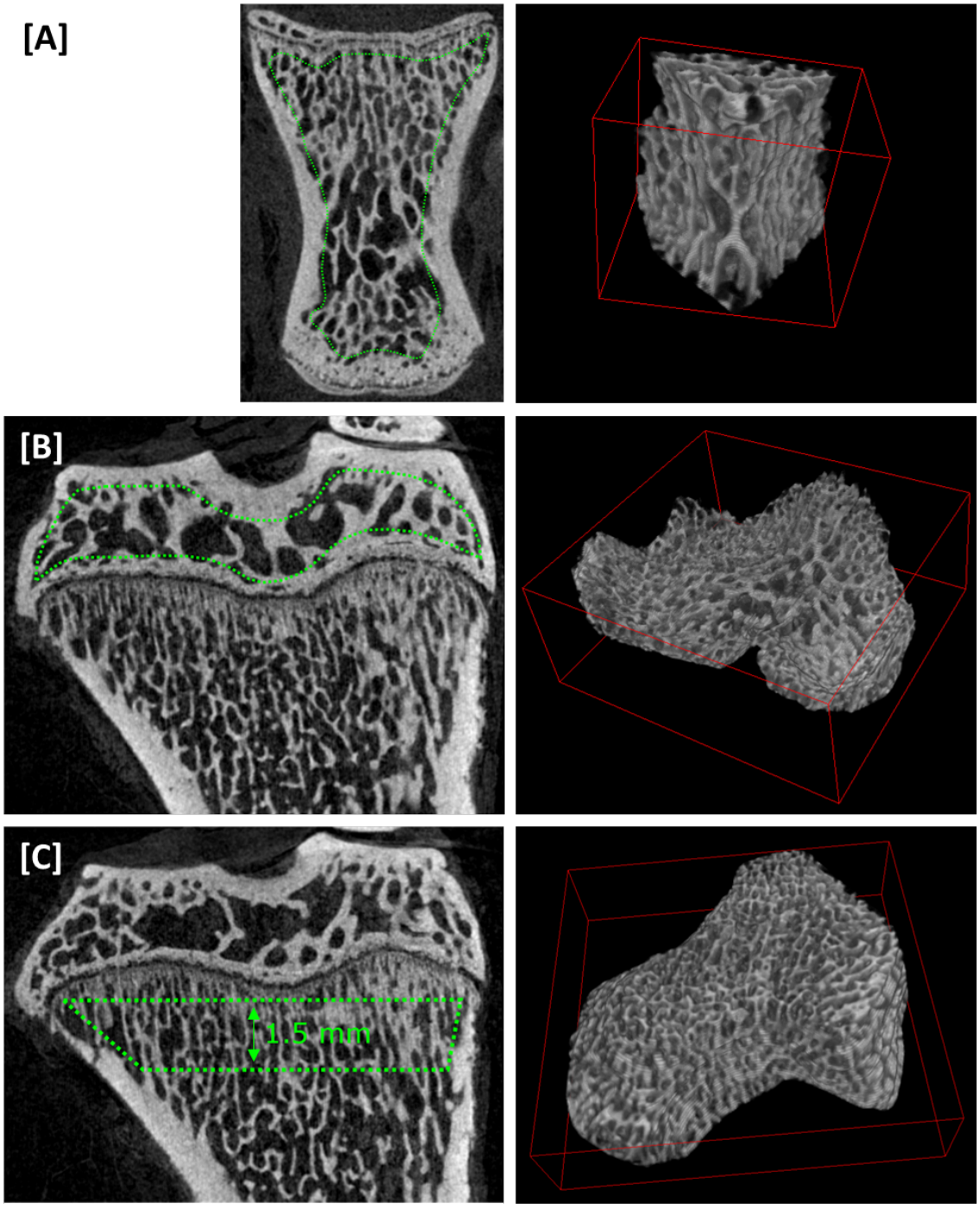

Figure 2. Representative example of the iterative curve fitting approach with both experimental (blue) and fitted model (red) curves plotted.

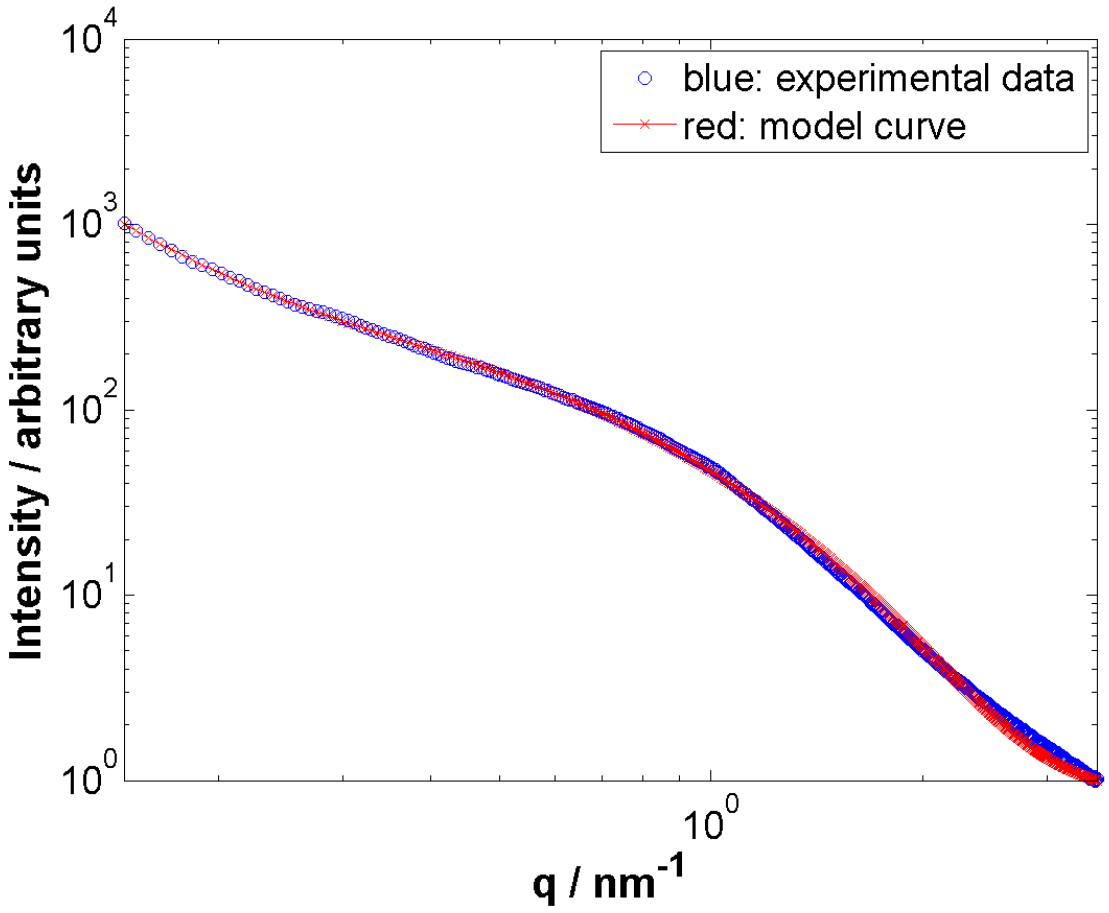

Figure 3. Representative μCT scans of Control and OVX L2 vertebral bodies highlighting the extent of osteoporotic trabecular degradation.

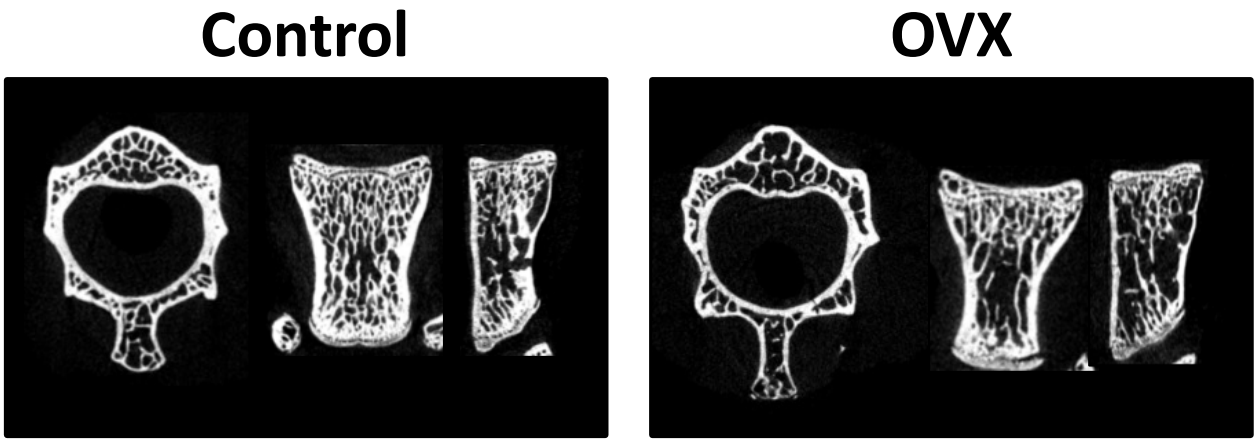

Figure 4. μCT analysis of control and OVX trabeculae in the L2 vertebral body, the tibial epiphysis and the the tibial metaphysis. BV/TV, Tb.N, Tb.Sp, Tb.Th, SMI and DA denote the bone volume fraction, trabecular number, trabecular separation, trabecular thickness, the structure model index and degree of anisotropy, respectively. (* $p < 0.05$, ** $p < 0.01$)

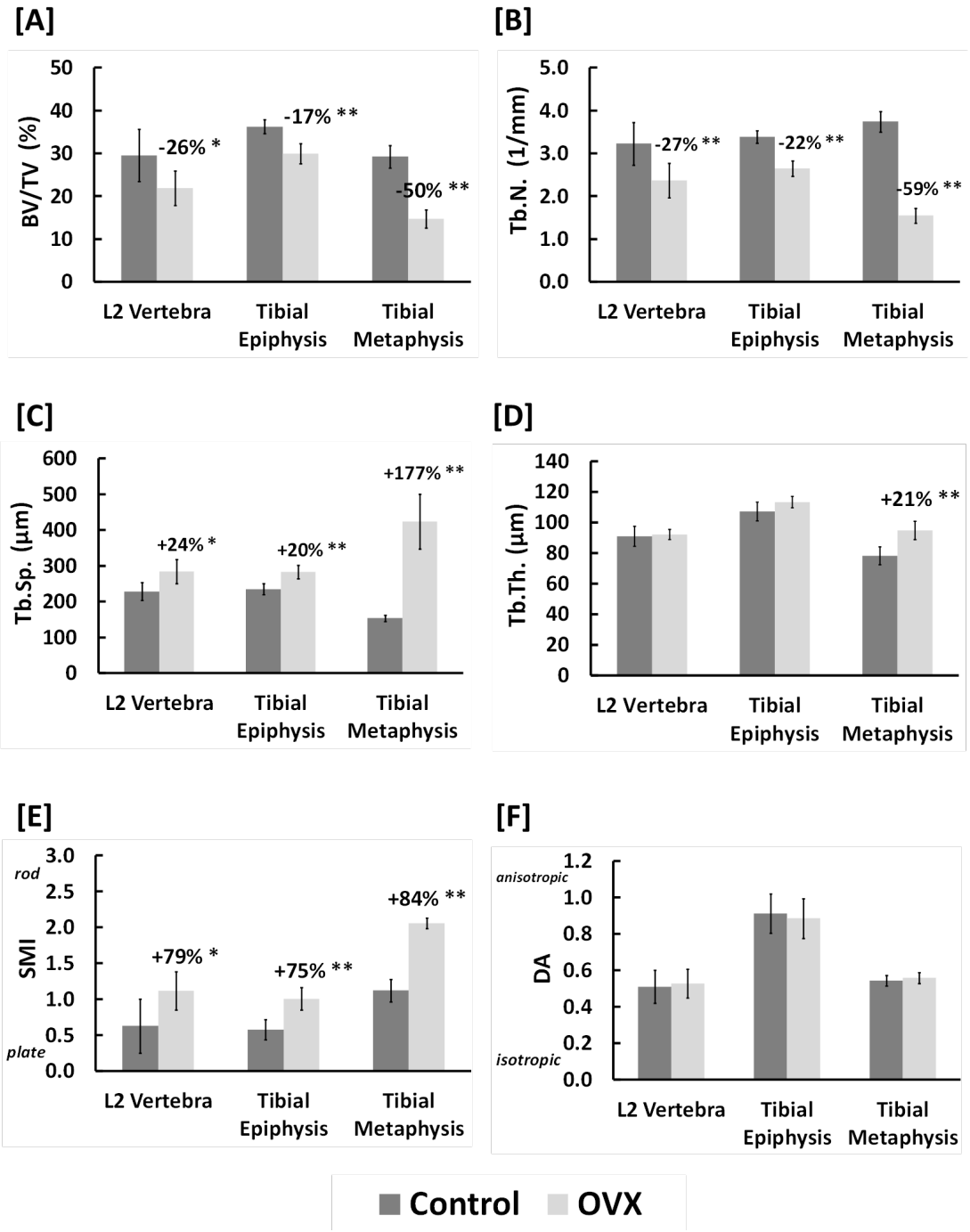

Figure 5. FTIR spectral parameters acquired in the proximal epiphysis of control and OVX tibiae. (* $p < 0.05$)

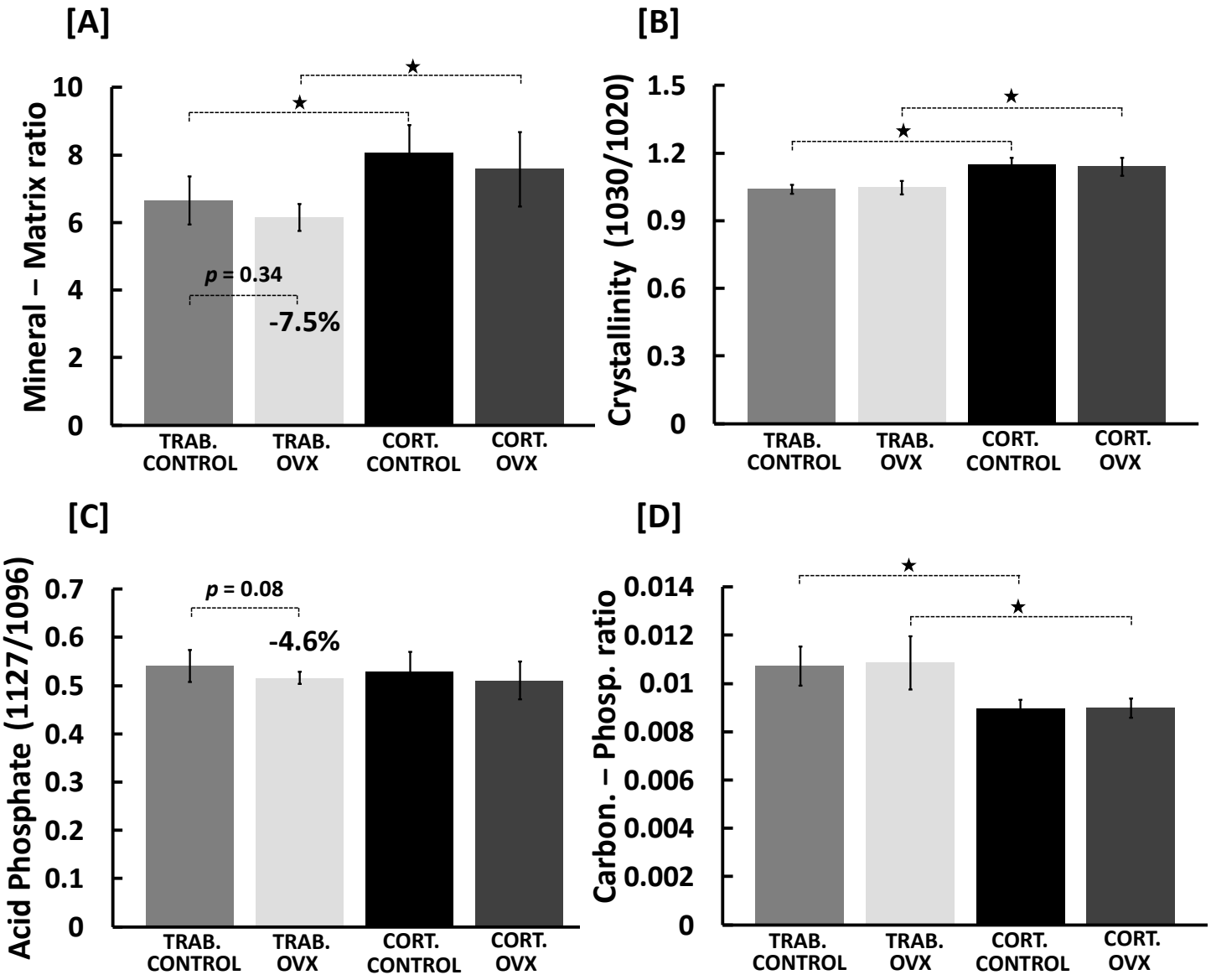

Figure 6. SAXS mineral plate thickness determined at the L2 lumbar vertebra and the proximal tibial metaphysis using both the curve fitting and Fratzl. approaches. (* $p < 0.05$)